Traumatic brain injury enhances the intrinsic excitation and excitatory transmission of granule cells

Joanna Danielewicz1,3*, Nerea Llamosas*1, Irene Dura1,4, Diego Martin Mateos1,2,# Juan Manuel Encinas1,4,5†
1 Achucarro Basque Center for Neuroscience, Leioa, Bizkaia, Spain
2 Consejo Nacional de Ciencia y Técnica (CONICET), Santa Fe, Argentina
3 BCAM Basque Center for Applied Mathematics, Bilbao, Bizkaia, Spain
4 University of the Basque Country (UPV/EHU), Leioa, Bizkaia, Spain
5 Ikerbasque, The Basque Science Foundation, Bilbao, Bizkaia, Spain
* Equal contribution
# Co-corresponding and co-last author
† JM.Encinas@achucarro.org

Abstract

Traumatic brain injury (TBI) is a leading cause of morbidity and mortality worldwide, affecting millions of people each year. TBI can lead to a wide range of physical and cognitive impairments. It is also known to impact on neuronal excitability and synaptic functions. Although hippocampal impairments have been widely described following TBI, the specific effects on dentate gyrus (DG), which act as “gatekeeper” of hippocampal information processing and as a filter of excessive or aberrant input activity, remains to be fully elucidated. In this study we investigated the effects of controlled cortical impact (CCI), as a model of TBI, on the excitability of granule cells and excitatory postsynaptic transmission in the DG at three different time periods, 3 days, 15 day and 4 months after the injury. Our results indicate TBI does not provoke changes in passive membrane properties of granule cells. By applying dimensionality reduction analysis of action potential properties, we were able to identify the variables that exhibited significant short-medium and long-term changes. Indeed, we observed that half-width, amplitude and overshoot of action potential were greater in TBI cells at different time points. Conversely, duration of afterhyperpolarization was reduced compared to control cells. Lastly, although amplitude of sEPSC did not show differences among groups at any time point, significant changes in frequency of sEPCS were observed in TBI cells at different time points, which did not follow the same temporal evolution as control animals. These findings indicate that at the long term TBI increases the intrinsic excitation of granule cells and excitatory synaptic activity of the DG.

1. Introduction

Traumatic brain injury (TBI) is a major cause of morbidity and mortality worldwide, affecting millions of people each year. TBI leads to diverse histopathological and behavioral consequences that begin shortly after the trauma (hours to days) and persist chronically (weeks, months, and years after injury). Following an initial insult, secondary damage occurs and involves local inflammation, excitotoxicity and other long – term changes that are triggered by the initial trauma (Girgis et al., 2016; Krishnamurthy & Laskowitz, 2016; Mengel et al., 2010). Even when brain trauma is mild, many individuals suffer from neuropsychological impairments such as memory loss, learning deficits, long – term disabling changes in cognition, sensorimotor function and personality (Corrigan et al., 2010; McKinlay et al., 1981; Schalén et al., 1994; Tate & Broe, 1999). Studies suggest that the hippocampus is particularly vulnerable to TBI. It has been observed that the hippocampus undergoes similar neuropathological changes in humans after closed – head injury and in animal experimental injury models of TBI (Isoniemi et al., 2006; McCarthy, 2003; Saatman et al., 2006). The pathologies in the hippocampus play a leading role in the disturbance of learning, memory, and higher cognitive function (Pullela et al. 2006). In fact, hippocampal neuronal loss accompanies >80% of fatal TBI and apoptotic events in the hippocampus can be observed up to 12 months following TBI (Chirumamilla et al., 2002; Dash et al., 2001; Pullela et al., 2006). Within the hippocampus, the dentate gyrus (DG) acts as a “gatekeeper” and a filter of excessive or aberrant input activity. It is believed that the filtering abilities of the DG are consequence of three main mechanisms: (1) the intrinsic membrane properties of granule cells (GCs) that tend to resist excessive excitation; (2) interconnections between GCs that impedes synchronization since neurons firing inappropriately cannot easily transmit this overexcitation to neighboring cells and (3) surrounding inhibitory interneurons and synaptic inhibitory efficacy (Claiborne et al., 1986; Fricke & Prince, 1984; Sloviter, 1994). DG function is directly determined by a delicate balance between neuronal excitation and inhibition and TBI can cause changes of this state of equilibrium. Therefore, this brain region plays a pivotal role in the consequences of traumatic brain injury. While significant cell death has been observed in the hilar region, the preferential survival of excitatory neurons has not been reported (Bonislawski et al., 2007; Lowenstein et al., 1992; Toth et al., 1997). Studies on the electrophysiological properties of the DG have consistently shown that TBI leads to increased DG excitability in rodents, effectively reducing its filtering capacity. It has been reported that DG hyperexcitability could result from either increased excitability of surviving granule cells, decreased synaptic inhibitory efficacy and/or increased synaptic excitatory efficacy (Bonislawski et al., 2007; Gupta et al., 2012; Santhakumar et al., 2000; Witgen et al., 2005). However, the exact consequences of TBI and the corresponding loss and/or the survival with modified electrophysiological properties, and of glutamatergic granule cells as the main components of the DG’s neuronal network are not fully understood. This study was carried out to determine the short-, medium- and long-term effects of controlled cortical impact (CCI), as a model of TBI, on the excitability of granule cells and excitatory postsynaptic transmission in the DG.

2. Materials and Methods

Animals and treatment

8 weeks old C57BL/6 mice were used for all procedures. Mice were housed at constant humidity and temperature with a 12-h light/dark cycle with food ad libitum. All experimental procedures were approved by the University of the Basque Country (EHU/UPV) Ethics Committee (Leioa, Spain) and the Comunidad Foral de Bizkaia (CEEA: M20/2015/236).
The animals were randomly assigned to the TBI, Sham or control group. TBI mice model was established with a controlled cortical impact (CCI) method (TBI 0310, Precision Systems and Instrumentation). Briefly, mice were anesthetized with ketamine and fixed on stereotaxic apparatus. A midline incision was made to expose the skull. An approximate 4-mm craniotomy was performed over the left parietotemporal cortex using a motorized drill. The CCI was centered a 2.5-mm lateral to the midline and a 0.5-mm anterior to bregma and was conducted with a 30-mm flat-tip impounder (velocity-5.5 m/s; duration-600 ms; depth-1 mm). After CCI, the scalp incision was sutured, and the mice were placed on a heating pad until anesthesia recovery. Sham mice received all these procedures, except for CCI. Control group of animals was subjected only to ketamine anesthesia.

Preparation of brain slices
Brain slices were prepared at 3 different time points after the TBI/Sham surgery. Their brains were quickly removed and placed in ice-cold artificial cerebrospinal fluid (ACSF) containing (in mM): 92 NMDG, 2.5 KCl, 0.5 $CaCl_2$, 10 $MgSO_4$, 1.25 NaH_2PO_4, 30 $NaHCO_3$, 20 HEPES, 5 Na- ascorbate, 3 Na-pyruvate, 2 Thiourea and 25 D-glucose (pH 7.3 – 7.4; 300 – 310 mOsm) and bubbled with the mixture of 95% O2–5% CO2. Coronal slices (thickness = 250 µm) containing DG were cut from hemisphere ipsilateral to the TBI/Sham surgery using a vibrating microtome (Leica VT1000). Slices were stored submerged at room temperature for recovery.

Whole-cell recording of action potentials and spontaneous excitatory postsynaptic currents from granule cells
After 1-1.5 h individual slices were placed in the recording chamber mounted on the stage of Scientifica microscope with 40x water immersion lens and superfused at 3 ml/min with warm (32 ± 0.5 °C), modified ACSF of the following composition (in mM): 124 NaCl, 4.5 KCl, 1.25 NaH_2PO_4, 26 $NaHCO_3$, 1 $MgSO_4$ * 7 H_2O, 1.8 $CaCl_2$, and 10 D-glucose (pH 7.3-7.4; 300-310 mOsm), bubbled with the mixture of 95% O2–5% CO2. Recording micropipettes were pulled from borosilicate glass capillaries (Science Products) using the PC-100 Nareshige puller. The pipette solution contained (in mM): 125 K-gluconate, 20 KCl, 2 MgCl2, 10 HEPES, 4 Na2-ATP, 0.4 Na-GTP, 5 EGTA (pH 7.3-7.4; 295-305 mOsm,). Pipettes had open tip resistances of approx. 7-9 MΩ. The calculated liquid junction potential using this solution was 13.1 mV, and data were corrected for this offset. Signals were recorded using Axon MultiClamp 700B amplifier (Molecular Devices), filtered at 2 kHz, and digitized at 20 kHz using Digidata 1550A (Molecular Devices) interface and Clampex 10 software (Molecular Devices, USA).
Cell access was obtained in the voltage-clamp mode and Resting Membrane Potential (RMP) was measured immediately upon break-in in the current-clamp mode by setting the clamp current equal to zero. The firing characteristics of the recorded cells was assessed using intracellular injections of rectangular current pulses of increasing amplitude (range: - 200 pA to + 200 pA; ΔI = 20 pA; duration: 400 ms) in current-clamp mode. The first action potential (AP) that was generated with the use of this current steps

protocol was used in further analysis of AP properties. For each cell, the relationship between injected current intensity and the number of AP was plotted. Evaluated AP properties were: voltage displacement from RMP to AP threshold (ΔVt), AP amplitude (AP amp), AP duration (AP dur) at 50% repolarization, AP maximum rise slope (AP max rise), AP maximum decay slope (AP max decay), afterhyperpolarization amplitude (AHP amp), and AHP duration (AHP dur) at 50% of decay back to RMP. The membrane input resistance (R_{in}) was determined from the slope of the current–voltage relationship. Membrane time constant *tau* was estimated by fitting the decay phase of the voltage phase to a standard exponential equation. Spontaneous excitatory postsynaptic currents (sEPSCs) were recorded as inward currents from neurons, which were voltage-clamped at -86 mV and synaptic events were recorded for 3 min for each neuron. Only cells with stable access resistance were accepted for the data analysis. Spontaneous EPSCs were detected off-line and analyzed using the Mini Analysis software (Synaptosoft, USA). Individual recorded traces were searched for peak currents using the automatic detection protocol. The average baseline current was calculated for an interval between 3 and 5 ms before the peak, the threshold amplitude for EPSC detection was set to 4 pA. Afterward recordings were inspected manually for correctness.

Principal component Analysis (PCA)

PCA, a widely used dimensionality reduction technique in data analysis, is a powerful tool for understanding and simplifying complex datasets with many features, as in this case. It provides a concise representation of the data while preserving maximum information. PCA identifies principal components (PCs), which are linear combinations of the original features. Each principal component captures a certain amount of variance in the data. Typically, the original principal components capture the majority of the variance, facilitating dimensionality reduction (Jolliffe & Cadima, 2016).

However, when applying PCA, it is crucial to determine how much of the variation in the data is explained by each principal component. A commonly used tool to achieve this is the cumulative explained variance ratio (CEVR). This metric is the cumulative sum of the explained variance of each principal component included in the analysis in turn. The CEVR proves to be instrumental in discerning the total variance retained as additional principal components are included. It helps to capture the trade-off between dimensionality reduction achieved by using fewer components and the retention of information from the original dataset.

Furthermore, we are interested in identifying the variables that contribute most to the components in the PCA analysis. For this purpose, we extract the principal loadings, which are essentially the top eigenvectors of the covariance matrix in the PCA algorithm.

In our study, we used PCA to reduce the dimensionality of the entire data set, focusing on passive membrane properties. Two principal components were obtained to facilitate comparisons between three different time points. In addition, we examined the three highest loadings to identify the original measures that were most influential in this comparative analysis.

Statistical analysis

Statistical analysis was performed using GraphPad Prism 9 (GraphPad Software) or Phyton (Python Software Foundation). All data sets were tested for deviation from normal distribution (D'Agostino). Data were analyzed using either a one – way ANOVA or two – way ANOVA. Post – hoc analysis for ANOVA was conducted using Tukey's test. For data that were not normally distributed, nonparametrical Kruskal-Wallis test was performed followed by Dunn´s multiple comparison test. Cumulative probsability distribution was compared using Kolmogorov–Smirnov's test). The level of statistical significance was set at $p < 0.05$.

3. Results

To investigate whether traumatic brain injury (TBI) modifies membrane properties of the DG granule neurons, comparisons were made between cells from TBI mice and those obtained from aged-matched Sham and control animals at 3 different timepoints (3 days, 15 days and 4 months) after the surgery. Resting membrane potential, membrane constant *tau* and membrane input resistance values in TBI and Sham groups remained similar to those in control any time point (Fig.1A-C), demonstrating that passive membrane properties were unaltered by the interventions. Next, we sought to determine whether TBI affects the intrinsic excitability of granule cells. For this purpose, we injected somatic current pulses of increasing intensity and examined the relationship between current pulses and the action potentials (AP) elicited. Compared to controls, neurons from TBI group exhibited similar AP generation in response to a range of current pulses (Fig. 1E-H). Consistent with this finding, rheobase was comparable in neurons from control and TBI mice (Fig. 1I-K), demonstrating that same amount of current is needed to induce a single AP in these neurons compared to controls. Unlike TBI, AP generation in Sham group was decreased compared to control at short- and medium term, but not long-term. At long-term, AP generation in Sham group was only reduced when compared to TBI (Fig. 1E-H) Rheobase Sham values, however, remained similar to those in control and TBI cells at the three time points (Fig. 1I-K). Taken together these results show that that neither TBI nor Sham surgery have long-term effects on passive membrane properties and threshold for AP generation of DG granule cells.

To investigate the effect of traumatic brain injury (TBI) on AP properties, we performed a detailed analysis of evoked AP waveforms. We calculated a total of 16 measurements, including amplitude, duration and velocity, from different fractions of the AP elicited by current-induced spiking responses in the three groups at three time points. Due to the high dimensionality of the data, we chose to use a dimensionality reduction method, specifically Principal Component Analysis (PCA). We decided to focus on the two primary components and compared the three groups at different time intervals (Fig. 2A-C). For day 3, a pronounced increase in the variance of Principal Component 1 (PC1) was observed in the Control and Sham states compared to the TBI values (Fig. 2A, D). However, no significant changes were observed between the values of these three groups in Principal Component 2. On day 15, we observed a similar trend for PC1 as on day 3, where the variance for TBI is lower than for Control and Sham (Fig. 2 B, E). In contrast, for PC2, TBI values were significantly higher than those of Control and Sham. Looking at month 4, the differences in PC1 between TBI and the other conditions are

less pronounced, and no significant changes are observed between the three conditions for PC2 (Fig. 2C, F).

Given that most of the variance captured by principal component 1 and 2 were features related to duration and amplitude of different AP fractions (Fig. 2G), we compared AP half-width, AP duration, AP overshoot and afterhyperpolarization (AHP) duration among groups at the three different time points (Fig. 3A). TBI significantly increased AP half-width 15 days after the surgery, although no early or sustained changes were otherwise observed (Fig. 3B). TBI cells showed a greater AP amplitude at day 3 and 15, but not 4 months after the surgery. This increased AP amplitude was also observed in Sham group at day 15. Again, these changes were no longer visible 4 months after the intervention (Fig. 3C). AP overshoot refers to the fraction of AP amplitude that happens when membrane potential raises above 0 and it is therefore closely correlated to AP amplitude. Thus, similar results were obtained when analyzing AP overshoot among groups at the different time points. At day 3 and 15 after the surgery, AP of TBI and Sham cells showed a statistically greater overshoot as compared to control values (Fig. 3D). This effect was transient as no sustained differences were found 4 months after the intervention. Nevertheless, we observed a long-term effect of TBI on AHP duration. TBI significantly decreased the duration of the AHP of granule cells at the short and long-term, and this effect was visible when compared to both control and Sham values (Fig. 3E). The impairments in AP properties were also present in other spiking features (Suppl. 1). Shortly after the surgery, TBI did not remarkably change any property, with the exception of a slight but significant decrease and increase in AHP decay time and time for 1st AP, respectively (Suppl. 1A, E). At day 15, TBI caused a reduction in AHP amplitude and voltage displacement and an increase rise slope and membrane threshold (Suppl. 1C, E, G, H). At the long term, TBI caused a decrease in AHP decay time and membrane threshold (Suppl. 1F-G). These results suggested that TBI diminishes the function of hyperpolarizing ion channel currents at the long-term.

We next sought to explore the short- medium- and long-term impact of TBI on the spontaneous excitatory transmission (sEPSC) of granule cells. However, synaptic activity undergoes biological changes over the course of time and this could be a confounding factor in the study. To test this, we first determined the evolution of spontaneous activity levels within each group.

Measurements of frequency of sEPSC in control granule cells indicated that there was a nonsignificant decline at day 15 compared to day 3 and a significant decrease at month 4 compared to day 15, mostly ascribed to the physiological course of excitatory transmission over the time. This observation, however, was not noticed in Sham and TBI groups (Fig. 4A-C). In fact, frequency of sEPCS in TBI group underwent a biphasic change of opposing effects: first a substantial reduction from day 3 to day 15 and later a marked increase from day 15 to 4 months after surgery. Sham group showed the same tendency as control, although the reduction in sEPSC frequency was not significant for this group (Fig. 4A-D)

Once the time course profile of sEPSC frequency was determined for all groups, we next investigated whether frequency of sEPSC was different in TBI and/or Sham compared to control at the three different time points.

Three days after the surgery, TBI and Sham granule cells showed similar sEPSC frequency values and cumulative probability plot compared to control mice (Fig. 5A-B). However, at day 15, there was a clear deviation in TBI group and consequently, cumulative probability distribution was significantly shifted to the right and sEPSC frequency was statistically decreased compared to control cells (Fig. 5C-D). Lastly, 4 months after the surgery TBI caused a marked increase in sEPSC frequency also shown in the shift to the left of cumulative probability distribution of inter-event intervals (Fig. 5E-F). Regarding frequency of sEPSC in Sham cells, no differences were observed when compared to control and TBI at any time point (Fig. 5A-C).

Lastly, as we did with frequency of sEPSC, we examined the temporal evolution of amplitudes of sEPSC. sEPSC amplitude values remained unaltered over the time in the three experimental groups (Fig. 6A and Suppl. 2A-C). Additionally, neither Sham nor TBI altered sEPSC amplitude at any time point (Fig. 6B-D), meaning that the effect of TBI on excitatory transmission of granule cells is restricted to frequency of spontaneously occurring events and pointing out to the involvement of presynaptic mechanisms.

4. Discussion

It has been established that early post-traumatic period is crucial in determining the outcome in head trauma in humans (Lam, 1997), therefore majority of animal studies are focused on short-term effects and are geared toward preventing TBI-induced changes by intervening within the first hours to days after injury. However, the electrophysiological, anatomical and behavioral consequences of TBI can be developing over long period of time even up to several months after the initial trauma. In our study we decided to examine both short-term as well as long-term effects in order to observe temporal dynamics of changes induced by TBI in DG electrophysiology.

The results of our study indicate that TBI does not affect passive membrane properties over time, as RMP, input resistance and membrane time constant tau remained unchanged at all of the experimental timepoints, which is in agreement with other findings (Gupta et al., 2012; Logue et al., 2016). As we mentioned earlier (see introduction) increased excitability of neurons is the most commonly reported outcome of TBI. However, our results indicate that the generation of action potentials in response to current pulses remained unaffected by TBI when compared with control animals, moreover we have not observed any significant changes in rheobase at any given timepoint leading to a general conclusion that our experimental model of TBI does not affect excitability of GCs, unlike in other findings. This discrepancy could be caused by using a different TBI method, the severity of the trauma or simply by a different electrophysiological approach(Corrubia et al., 2023; Gupta et al., 2012; Witgen et al., 2005). The analysis of action potential waveforms revealed TBI-induced alterations in active membrane properties. Granule cells in injured animals exhibited larger AP amplitude and AP overshoot 3 days and 15 days after the traumatic event. Interestingly, similar effects were observed in Sham animals 15 days post-surgery when compared to controls. Such outcomes would be expected to be also accompanied by lower spike threshold and changes in AP max rise time and max decay time slopes, however in our study we have not observed these alterations 3 days post-TBI. Moreover, shortly after TBI, AHP duration and AHP decay are decreased when compared to both Sham and control animals. 15 days after TBI, changes in AP amplitude were accompanied by a reduction in AHP amplitude and voltage displacement, moreover an increase in AP rise time slope and membrane threshold were also present. The increasement of the AP

amplitude was a transient effect of the injury as no significant differences were found 4 months after the surgery. In long-term manner, similarly to what we observed on day 3, TBI affected both the duration and the decay of AHP as these parameters were significantly reduced when compared to Sham and controls. Similar changes in AP amplitude were observed in pyramidal neurons recorded in layer V of somatosensory cortex (Greer et al., 2012) and in CA1 hippocampal neurons shortly after traumatic brain injury (Logue et al., 2016). Logue et.al, alongside increased AP amplitude have not reported any significant changes in AHP parameters, however similarly to our observations, no changes in frequency of AP firing and rheobase were detected 7 days after repetitive closed head injury.

In our study, TBI-induced alterations in active membrane properties without significantly affecting passive membrane properties could indicate that the nature of these alterations most likely lays in changes in somatic and/or perisomatic voltage-gated channels. TBI can indeed modify the density of channels and their functional kinetics, affecting the generation and modulation of action potentials. Voltage-gated sodium channels (VGSCs) are vital for generating and propagating action potentials in neurons. In mammals, nine Nav α subunit genes have been identified, among which Nav1.1, Nav1.2, Nav1.3, and Nav1.6 are mainly expressed in the central nervous system (Harms et al., 2017). Previous studies have reported that VGSCs regulate Na+ permeability across the membrane and are sensitive to traumatic brain injury. It has been shown that the protein and mRNA expression of Nav1.3 is significantly increased in rodent and in human TBI model and it's correlated with severity of the brain trauma. Additionally, it was revealed that blocking the elevated Nav1.3 could enhance recovery from TBI (X. Huang et al., 2014; X.-J. Huang et al., 2022; Wolf et al., 2001; Zhang et al., 2023). An upregulation of the expression of both mRNA and protein levels of Nav 1.6 channel was also shown shortly after TBI in the rat hippocampus (Mao et al., 2010). Small-conductance calcium-activated potassium channels (SK channels) play a significant role in shaping the AHP. SK channels are activated by a rise in intracellular Ca2+ and they are thought to not only contribute to the AHP, but they may also play an important role in regulating neuronal excitability and synaptic transmission (Faber & Sah, 2007). Recent studies have shown that activation of SK channels may play a very important role in neuroprotective mechanisms against neuronal injury after a stroke or against TBI-induced neuroinflammation. In fact pharmacological agonists of SK channels are considered to have strong therapeutic potential against TBI-induced damages (Chen et al., 2019; Dolga et al., 2011). It is therefore probable that a reduction in SK channel activity could explain the effects of TBI observed in our study. First, SK channels contribute to the medium-duration AHP (mAHP) phase and the slow-duration AHP (sAHP) phase, therefore a reduction in SK channel activity may lead to a shorter duration and decreased AHP decay observed here. Second, a reduction in SK channel activity can result in a decrease in the overall potassium efflux, leading to a smaller AHP amplitude.

Voltage-clamp recordings of spontaneous current activity provided further insights into the TBI-induced changes in DG electrophysiology. It has been demonstrated that both sEPSC frequency and amplitude can be affected by age in striatal neurons and in pyramidal layer V cells (Wong et al., 2000), therefore we decided to first determine if similar effects are occurring in our study within each group. We have observed a steady, significant decline in sEPSC frequency in the control group and a similar, but insignificant trend in Sham animals. Interestingly, after TBI we have observed a biphasic change with opposite outcome. Initially, a significant decrease of sEPSC frequency was present at day 15 when compared to day 3, however later on at 4 month time point sEPSC

frequency was significantly enhanced. Furthermore, a comparison of sEPSC frequency between the groups revealed that TBI affects current activity in an opposite manner over time. We observed no effects of TBI on current activity 3 days after the trauma, however the decrease in the sEPSC frequency at day 15 and a significant increase later were present. Witkowski and colleagues reported a very little effect on mean postsynaptic currents frequency, suggesting that a relatively minor impact on synaptic transmission only 48 hour after the injury (Witkowski et al., 2019). Interestingly, 14 days after the repetitive head trauma decreased sEPSC frequency was shown in CA 1 pyramidal cells (Langlois et al., 2022), however in the studies reported by Louge and colleagues the same TBI procedure caused an opposite effect (Logue et al., 2016). The difference between those studies was the earlier time point of electrophysiological recordings. This suggests that the same TBI procedure can in fact affect sEPSC frequency differently in a time-related manner. It has been reported that in the chronic period (3-5 weeks), TBI resulted in an increase of spontaneous synaptic excitation in layer V pyramidal neurons (Cantu et al., 2015; Koenig et al., 2019) supporting our findings at the 4 month time point. In agreement with our findings, no changes in the sEPSC amplitude were observed in these studies, suggesting that most likely presynaptic mechanisms, such as increased glutamate synthesis, vesicular loading, or release efficiency may contribute to elevated sEPSC frequency. Indeed, Cantu and colleagues reported enhanced glutamate signaling in deep cortical layers near the site of injury.

Many other mechanisms contribute to TBI pathophysiology including increased inflammation. It has been shown that TBI triggers an immediate immune response that causes migration if inflammatory cells into the brain and activation of residing microglia (Cederberg & Siesjö, 2010; Fan et al., 1995; Helmy et al., 2011). This response is designed to trigger compensation mechanisms that would minimize neuronal damage and start healing processes; however, it can also become maladaptive if the trauma is severe enough. We believe that neuroinflammation triggered by TBI is contributing to the changes observed in our study, moreover an inflammatory reaction could also be responsible for the outcomes of Sham surgery. Since majority of commonly applied TBI models require a craniotomy, Sham animals are also undergoing this procedure. Even in the absence of the specific manipulation like cortical impact, the surgical procedure itself can induce stress and inflammation which in turn may affect neuronal excitability and lead to changes in active membrane properties.

In conclusion, TBI-induced changes in active membrane properties and excitatory synaptic currents observed in this study suggest that neuronal network remodeling in the dentate gyrus is a dynamic process that commences shortly after the trauma and persist for several months.

Bibliography

Bonislawski, D. P., Schwarzbach, E. P., & Cohen, A. S. (2007). Brain injury impairs dentate gyrus inhibitory efficacy. *Neurobiology of disease*, *25*(1), 163-169. https://doi.org/10.1016/j.nbd.2006.09.002

Cantu, D., Walker, K., Andresen, L., Taylor-Weiner, A., Hampton, D., Tesco, G., & Dulla, C. G. (2015). Traumatic Brain Injury Increases Cortical Glutamate Network Activity by Compromising GABAergic Control. *Cerebral Cortex (New York, N.Y.: 1991)*, *25*(8), 2306-2320. https://doi.org/10.1093/cercor/bhu041

Cederberg, D., & Siesjö, P. (2010). What has inflammation to do with traumatic brain injury? *Child's Nervous System*, *26*(2), 221-226. https://doi.org/10.1007/s00381-009-1029-x

Chen, T., Zhu, J., Hang, C.-H., & Wang, Y.-H. (2019). The Potassium SK Channel Activator NS309 Protects Against Experimental Traumatic Brain Injury Through Anti-Inflammatory and Immunomodulatory Mechanisms. *Frontiers in Pharmacology*, *10*. https://www.frontiersin.org/articles/10.3389/fphar.2019.01432

Chirumamilla, S., Sun, D., Bullock, M. R., & Colello, R. J. (2002). Traumatic brain injury induced cell proliferation in the adult mammalian central nervous system. *Journal of Neurotrauma*, *19*(6), 693-703. https://doi.org/10.1089/08977150260139084

Claiborne, B. J., Amaral, D. G., & Cowan, W. M. (1986). A light and electron microscopic analysis of the mossy fibers of the rat dentate gyrus. *The Journal of Comparative Neurology*, *246*(4), 435-458. https://doi.org/10.1002/cne.902460403

Corrigan, J. D., Selassie, A. W., & Orman, J. A. L. (2010). The epidemiology of traumatic brain injury. *The Journal of Head Trauma Rehabilitation*, *25*(2), 72-80. https://doi.org/10.1097/HTR.0b013e3181ccc8b4

Corrubia, L., Huang, A., Nguyen, S., Shiflett, M. W., Jones, M. V., Ewell, L. A., & Santhakumar, V. (2023). Early deficits in dentate circuit and behavioral pattern separation after concussive brain injury. *Experimental Neurology*, *370*, 114578. https://doi.org/10.1016/j.expneurol.2023.114578

Dash, P. K., Mach, S. A., & Moore, A. N. (2001). Enhanced neurogenesis in the rodent hippocampus following traumatic brain injury. *Journal of Neuroscience Research*, *63*(4), 313-319. https://doi.org/10.1002/1097-4547(20010215)63:4<313::AID-JNR1025>3.0.CO;2-4

Dolga, A. M., Terpolilli, N., Kepura, F., Nijholt, I. M., Knaus, H.-G., D'Orsi, B., Prehn, J. H. M., Eisel, U. L. M., Plant, T., Plesnila, N., & Culmsee, C. (2011). KCa2 channels activation prevents [Ca2+]i deregulation and reduces neuronal death following glutamate toxicity and cerebral ischemia. *Cell Death & Disease*, *2*(4), e147. https://doi.org/10.1038/cddis.2011.30

Faber, E. S. L., & Sah, P. (2007). Functions of SK channels in central neurons. *Clinical and Experimental Pharmacology & Physiology*, *34*(10), 1077-1083. https://doi.org/10.1111/j.1440-1681.2007.04725.x

Fan, L., Young, P. R., Barone, F. C., Feuerstein, G. Z., Smith, D. H., & McIntosh, T. K. (1995). Experimental brain injury induces expression of interleukin-1 beta mRNA in the rat brain. *Brain Research. Molecular Brain Research*, *30*(1), 125-130. https://doi.org/10.1016/0169-328x(94)00287-o

Fricke, R. A., & Prince, D. A. (1984). Electrophysiology of dentate gyrus granule cells. *Journal of Neurophysiology*, *51*(2), 195-209. https://doi.org/10.1152/jn.1984.51.2.195

Girgis, F., Pace, J., Sweet, J., & Miller, J. P. (2016). Hippocampal Neurophysiologic Changes after Mild Traumatic Brain Injury and Potential Neuromodulation Treatment Approaches. *Frontiers in Systems Neuroscience*, *10*, 8. https://doi.org/10.3389/fnsys.2016.00008

Greer, J. E., Povlishock, J. T., & Jacobs, K. M. (2012). Electrophysiological Abnormalities in Both Axotomized and Nonaxotomized Pyramidal Neurons following Mild Traumatic Brain Injury. *The Journal of Neuroscience*, *32*(19), 6682-6687. https://doi.org/10.1523/JNEUROSCI.0881-12.2012

Gupta, A., Elgammal, F. S., Proddutur, A., Shah, S., & Santhakumar, V. (2012). Decrease in Tonic Inhibition Contributes to Increase in Dentate Semilunar Granule Cell Excitability after Brain Injury. *The Journal of Neuroscience*, *32*(7), 2523-2537. https://doi.org/10.1523/JNEUROSCI.4141-11.2012

Harms, E., Stoetzer, C., Stueber, T., O'Reilly, A. O., & Leffler, A. (2017). Investigation into the role of an extracellular loop in mediating proton-evoked inhibition of voltage-gated sodium channels. *Neuroscience Letters*, *661*, 5-10. https://doi.org/10.1016/j.neulet.2017.09.039

Helmy, A., De Simoni, M.-G., Guilfoyle, M. R., Carpenter, K. L. H., & Hutchinson, P. J. (2011). Cytokines and innate inflammation in the pathogenesis of human

traumatic brain injury. *Progress in Neurobiology*, *95*(3), 352-372. https://doi.org/10.1016/j.pneurobio.2011.09.003

Huang, X., Li, W., Lin, Y., Feng, J., Jia, F., Mao, Q., & Jiang, J. (2014). Blockage of the Upregulation of Voltage-Gated Sodium Channel Nav1.3 Improves Outcomes after Experimental Traumatic Brain Injury. *Journal of Neurotrauma*, *31*(4), 346-357. https://doi.org/10.1089/neu.2013.2899

Huang, X.-J., Su, G.-J., Wu, C.-W., Sha, X.-S., Zou, J.-F., Liu, X.-S., Li, M., & He, Y. (2022). Knockdown of rno_circRNA_009194 Improves Outcomes in Traumatic Brain Injury Rats through Inhibiting Voltage-Gated Sodium Channel Nav1.3. *Journal of Neurotrauma*, *39*(1-2), 196-210. https://doi.org/10.1089/neu.2020.7520

Isoniemi, H., Kurki, T., Tenovuo, O., Kairisto, V., & Portin, R. (2006). Hippocampal volume, brain atrophy, and APOE genotype after traumatic brain injury. *Neurology*, *67*(5), 756-760. https://doi.org/10.1212/01.wnl.0000234140.64954.12

Jolliffe, I. T., & Cadima, J. (2016). Principal component analysis: A review and recent developments. *Philosophical Transactions. Series A, Mathematical, Physical, and Engineering Sciences*, *374*(2065), 20150202. https://doi.org/10.1098/rsta.2015.0202

Koenig, J. B., Cantu, D., Low, C., Sommer, M., Noubary, F., Croker, D., Whalen, M., Kong, D., & Dulla, C. G. (2019). Glycolytic inhibitor 2-deoxyglucose prevents cortical hyperexcitability after traumatic brain injury. *JCI Insight*, *5*(11), e126506, 126506. https://doi.org/10.1172/jci.insight.126506

Krishnamurthy, K., & Laskowitz, D. T. (2016). Cellular and Molecular Mechanisms of Secondary Neuronal Injury following Traumatic Brain Injury. En D. Laskowitz & G. Grant (Eds.), *Translational Research in Traumatic Brain Injury*. CRC Press/Taylor and Francis Group. http://www.ncbi.nlm.nih.gov/books/NBK326718/

Lam, A. M. (1997). Anesthetic Management of the Head-Injured Patient. En J. O. Johnson, R. J. Sperry, & T. H. Stanley (Eds.), *Neuroanesthesia: Papers presented at the 42nd Annual Postgraduate Course in Anesthesiology, February 1997* (pp. 139-151). Springer Netherlands. https://doi.org/10.1007/978-94-011-5774-2_10

Langlois, L. D., Selvaraj, P., Simmons, S. C., Gouty, S., Zhang, Y., & Nugent, F. S. (2022). Repetitive mild traumatic brain injury induces persistent alterations in spontaneous synaptic activity of hippocampal CA1 pyramidal neurons. *IBRO Neuroscience Reports*, *12*, 157-162. https://doi.org/10.1016/j.ibneur.2022.02.002

Logue, O. C., Cramer, N. P., Xu, X., Perl, D. P., & Galdzicki, Z. (2016). Alterations of functional properties of hippocampal networks following repetitive closed-head injury. *Experimental Neurology*, *277*, 227-243. https://doi.org/10.1016/j.expneurol.2015.12.019

Lowenstein, D. H., Thomas, M. J., Smith, D. H., & McIntosh, T. K. (1992). Selective vulnerability of dentate hilar neurons following traumatic brain injury: A potential mechanistic link between head trauma and disorders of the hippocampus. *The Journal of Neuroscience: The Official Journal of the Society for Neuroscience*, *12*(12), 4846-4853. https://doi.org/10.1523/JNEUROSCI.12-12-04846.1992

Mao, Q., Jia, F., Zhang, X.-H., Qiu, Y.-M., Ge, J.-W., Bao, W.-J., Luo, Q.-Z., & Jiang, J.-Y. (2010). The up-regulation of voltage-gated sodium channel Nav1.6 expression following fluid percussion traumatic brain injury in rats. *Neurosurgery*, *66*(6), 1134-1139; discussion 1139. https://doi.org/10.1227/01.NEU.0000369612.31946.A2

McCarthy, M. M. (2003). Stretching the truth. Why hippocampal neurons are so vulnerable following traumatic brain injury. *Experimental Neurology*, *184*(1), 40-43. https://doi.org/10.1016/j.expneurol.2003.08.020

McKinlay, W. W., Brooks, D. N., Bond, M. R., Martinage, D. P., & Marshall, M. M. (1981). The short-term outcome of severe blunt head injury as reported by relatives of the injured persons. *Journal of Neurology, Neurosurgery, and Psychiatry*, *44*(6), 527-533. https://doi.org/10.1136/jnnp.44.6.527

Mengel, B., Hunziker, A., Pedersen, L., Trusina, A., Jensen, M. H., & Krishna, S. (2010). Modeling oscillatory control in NF-κB, p53 and Wnt signaling. *Current Opinion in Genetics & Development*, *20*(6), 656-664. https://doi.org/10.1016/j.gde.2010.08.008

Pullela, R., Raber, J., Pfankuch, T., Ferriero, D. M., Claus, C. P., Koh, S.-E., Yamauchi, T., Rola, R., Fike, J. R., & Noble-Haeusslein, L. J. (2006). Traumatic injury to the immature brain results in progressive neuronal loss, hyperactivity and delayed cognitive impairments. *Developmental Neuroscience*, *28*(4-5), 396-409. https://doi.org/10.1159/000094166

Saatman, K. E., Feeko, K. J., Pape, R. L., & Raghupathi, R. (2006). Differential behavioral and histopathological responses to graded cortical impact injury in mice. *Journal of Neurotrauma*, *23*(8), 1241-1253. https://doi.org/10.1089/neu.2006.23.1241

Santhakumar, V., Bender, R., Frotscher, M., Ross, S. T., Hollrigel, G. S., Toth, Z., & Soltesz, I. (2000). Granule cell hyperexcitability in the early post-traumatic rat dentate gyrus: The «irritable mossy cell» hypothesis. *The Journal of Physiology*, *524 Pt 1*(Pt 1), 117-134. https://doi.org/10.1111/j.1469-7793.2000.00117.x

Schalén, W., Hansson, L., Nordström, G., & Nordström, C. H. (1994). Psychosocial outcome 5-8 years after severe traumatic brain lesions and the impact of rehabilitation services. *Brain Injury*, *8*(1), 49-64. https://doi.org/10.3109/02699059409150958

Sloviter, R. S. (1994). The functional organization of the hippocampal dentate gyrus and its relevance to the pathogenesis of temporal lobe epilepsy. *Annals of Neurology*, *35*(6), 640-654. https://doi.org/10.1002/ana.410350604

Tate, R. L., & Broe, G. A. (1999). Psychosocial adjustment after traumatic brain injury: What are the important variables? *Psychological Medicine*, *29*(3), 713-725. https://doi.org/10.1017/s0033291799008466

Toth, Z., Hollrigel, G. S., Gorcs, T., & Soltesz, I. (1997). Instantaneous perturbation of dentate interneuronal networks by a pressure wave-transient delivered to the neocortex. *The Journal of Neuroscience: The Official Journal of the Society for Neuroscience*, *17*(21), 8106-8117. https://doi.org/10.1523/JNEUROSCI.17-21-08106.1997

Witgen, B. M., Lifshitz, J., Smith, M. L., Schwarzbach, E., Liang, S.-L., Grady, M. S., & Cohen, A. S. (2005). Regional hippocampal alteration associated with cognitive deficit following experimental brain injury: A systems, network and cellular evaluation. *Neuroscience*, *133*(1), 1-15. https://doi.org/10.1016/j.neuroscience.2005.01.052

Witkowski, E. D., Gao, Y., Gavsyuk, A. F., Maor, I., DeWalt, G. J., Eldred, W. D., Mizrahi, A., & Davison, I. G. (2019). Rapid Changes in Synaptic Strength After Mild Traumatic Brain Injury. *Frontiers in Cellular Neuroscience*, *13*, 166. https://doi.org/10.3389/fncel.2019.00166

Wolf, J. A., Stys, P. K., Lusardi, T., Meaney, D., & Smith, D. H. (2001). Traumatic axonal injury induces calcium influx modulated by tetrodotoxin-sensitive sodium channels. *The Journal of Neuroscience: The Official Journal of the Society for Neuroscience*, *21*(6), 1923-1930. https://doi.org/10.1523/JNEUROSCI.21-06-01923.2001

Wong, T. P., Marchese, G., Casu, M. A., Ribeiro-da-Silva, A., Cuello, A. C., & De Koninck, Y. (2000). Loss of presynaptic and postsynaptic structures is accompanied by compensatory increase in action potential-dependent synaptic input to layer V neocortical pyramidal neurons in aged rats. *The Journal of*

Neuroscience: The Official Journal of the Society for Neuroscience, *20*(22), 8596-8606. https://doi.org/10.1523/JNEUROSCI.20-22-08596.2000

Zhang, D., Su, G. J., Wu, C. W., Zou, J. F., Wu, J. N., Deng, Y. H., & Huang, X. J. (2023). *Abnormal Changes in Voltage-Gated Sodium Channels Subtype Nav1.3 and Calmodulin-Dependent Protein Kinase Ii/Phosphorylation-Calmodulin-Dependent Protein Kinase Ii Pathway in Traumatic Brain Injury* (SSRN Scholarly Paper 4510761). https://doi.org/10.2139/ssrn.4510761

Figure legends

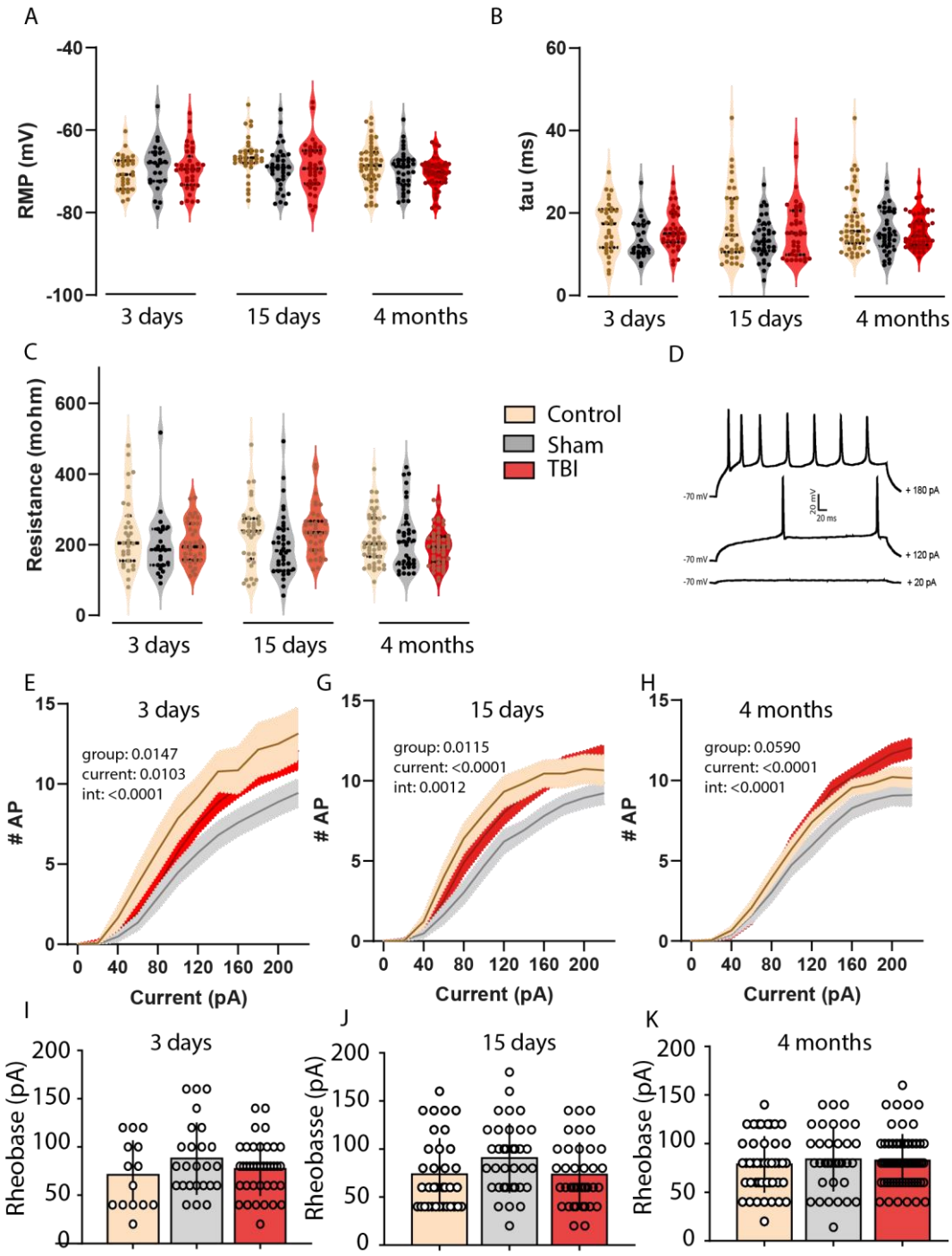

Figure 1. TBI does not alter membrane excitability in granule cells

(**A**) Resting membrane potential of control (orange), Sham (gray) and TBI (red) granule cells, 3 days (n=31 neurons from control; 24 from Sham and 37 from TBI) 15 days (n=36 neurons from control; 36 from Sham and 37 from TBI) and 4 months after the surgery (n=49 neurons from control; 36 from Sham and 52 from TBI). (**B**) *Tau* membrane constant of control, Sham and TBI granule cells. (**C**) Input resistance of granule cells from control, Sham and TBI groups. (**D**) Representative trace for membrane potential responses to current pulses from +20pA to +220 pA in steps of 20 pA (**E-G**) Input/output curves for control (orange), Sham (gray) and TBI (red) granule cell population at day 3 (E), day 15 (F) and 4 months (G) after the surgery (Two-way-ANOVA, group F (2, 74)= 4.472,p=0.0147, int F (22, 814)= 1.850, p=0.0103 for day 3; group F (2, 104)= 4.663,p= 0.0115, int F (22, 1144)= 2.192 p= 0,0012 for day 15; group F (2, 138)= 2.890,p= 0.0590, F (22, 1518)= 3.200 p< 0.0001 for 4 months).(**H-J**) Bar plots show rheobase from control,Sham and TBI groups at day 3 (H), day 15 (I) and 4 months (J) after the surgery. For A, B and C n=31 neurons from control; 24 from Sham and 37 from TBI at day 3; n=36 neurons from control; 36 from Sham and 37 from TBI at day 15; n=49 neurons from control; 36 from Sham and 52 from TBI at 4 months. For E to K n=14 neurons from control; 25 from Sham and 38 from TBI at day 3; n=35 neurons from control; 35 from Sham and 37 from TBI at day 15; n=43 neurons from control; 34 from Sham and 64 from TBI at 4 months. In violin plots dots represent individual cell values and dashed lines quartiles and medians. For line graphs area fill represents SEM. Circles in bar graphs represent cell values and bars represent mean ± SEM.

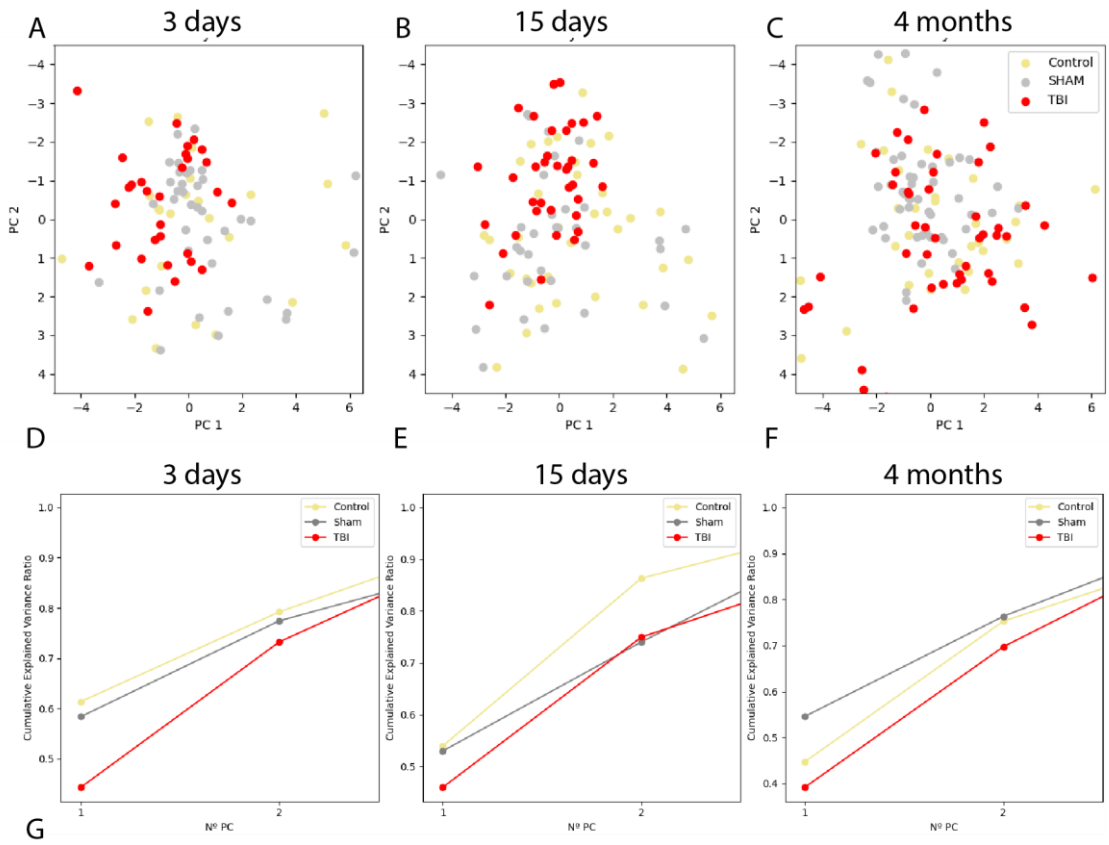

Day	PC	var1 name	var2 name	var3 name	var1 value	var2 value	var3 value
3d	1	Max decay slope (mV/ms)	AP over (mV)	Max rise slope (mV/ms)	0,42	0,42	0,41
3d	2	Threshold (mV)	ΔVt (mV) voltage displacement	Half width (ms)	0,52	0,46	0,42
15d	1	Max rise slope (mV/ms)	Max decay slope (mV/ms)	AP over (mV)	0,47	0,44	0,37
15d	2	ΔVt (mV) voltage displacement	AP Amplitude (mV)	AHP duration	0,41	0,41	0,39
4m	1	Max decay slope (mV/ms)	Max rise slope (mV/ms)	Half width (ms)	0,44	0,43	0,33
4m	2	AP Amplitude (mV)	AP over (mV)	AHP decay (mV*ms)	0,41	0,39	0,39

Figure 2. Principal Component Analysis (PCA) and Cumulative Explained Variance Ratio (CEVR) assessment of action potential features.

(**A-C**) Two-dimensional PCA plots illustrating the distribution of control (orange), Sham (gray), and TBI (red) granule cells at day 3 (A), day 15 (B), and 4 months (C). (**D-F**) Cumulative Explained Variance Ratio (CEVR) plots depicting the proportion of total variance explained by principal components for control (orange), Sham (gray), and TBI (red) granule cells at day 3 (D), day 15 (E), and 4 months (F). (**G**) Summary table presenting the loading variables with higher weights in Principal Component Analysis 1, 2, and 3 for day 3, day 15, and 4 months.

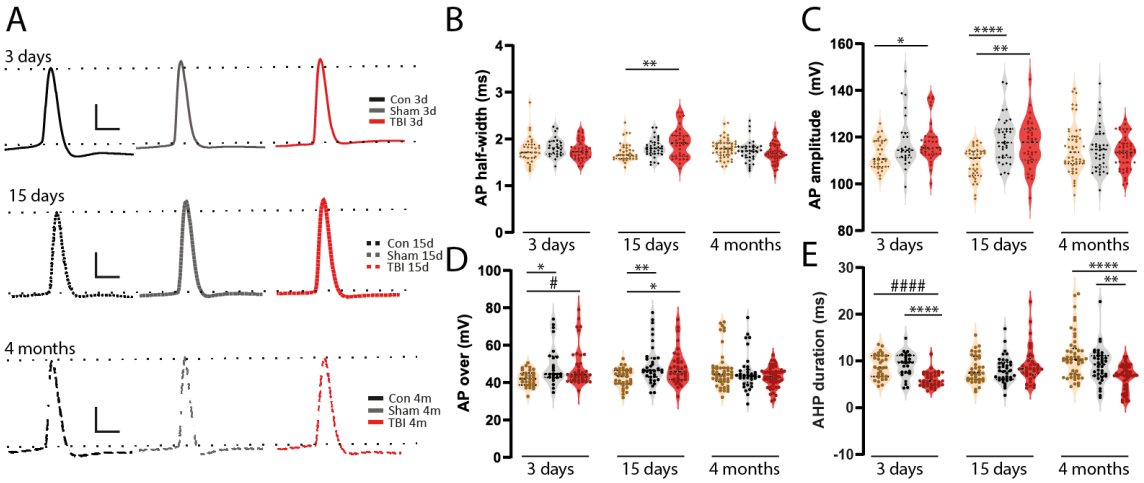

Figure 3. TBI affects action potential waveforms at short- medium- and long-term

(**A**) Examples of action potentials recorded 3 days, 15 days and 4 months after TBI/Sham surgery with a corresponding control (Scale bars: 20 mV, 5ms). (**B**) AP half-width in control (orange), Sham (gray) and TBI (red) groups at day3, day 15 and 4 months after the surgery (for day 15: Kruskal-Wallis test, H(2)= 9.241, p= 0.0098. ** p=0.0083 for TBI vs control in Dunn's multiple comparisons test). (**C**) AP amplitude in control (orange), Sham (gray) and TBI (red) groups at day3, day 15 and 4 months after the surgery (for day 3: Kruskal-Wallis test, H(2)= 7.176, p= 0.0277. *p=0,0292 for TBI vs control in Dunn's multiple comparisons test. For day 15: Kruskal-Wallis test, H(2)= 20.30, p <0.0001. **p=0.012 for TBI vs control and ****p<0.0001 for Sham vs control in Dunn's multiple comparisons test. (**D**) AP overshot in control (orange), Sham (gray) and TBI (red) groups at day3, day 15 and 4 months after the surgery(for day 3: Kruskal-Wallis test, H(2)= 9.544, p= 0.0085. *p= 0.0176 for Sham vs control, #p= 0,0311 for TBI vs control in Dunn's multiple comparisons test. For day 15: Kruskal-Wallis test, H(2)= 11.36, p= 0.0034. **p=0.0051 for Sham vs control and *p=0.0247 for TBI vs control in Dunn's multiple comparisons test. (**E**) AHP duration in control (orange), Sham (gray) and TBI (red) groups at day3, day 15 and 4 months after the surgery (for day 3: Kruskal-Wallis test, H(2)= 27.06, p<0.0001. ####p<0.0001 for TBI vs control and ****p= 0.0001 for Sham vs TBI in Dunn's multiple comparisons test. For 4 months: Kruskal-Wallis test, H(2)= 26.76, p< 0.0001. ****p<0.0001 for TBI vs control and **p=0.0035 for TBI vs Sham in Dunn's multiple comparisons test. n=31 neurons from control; 24 from Sham and 37 from TBI at

day 3; n=36 neurons from control; 36 from Sham and 37 from TBI at day 15; n=49 neurons from control; 36 from Sham and 52 from TBI at 4 months. Dots in violin plots represent individual cell values and dashed lines quartiles and medians.

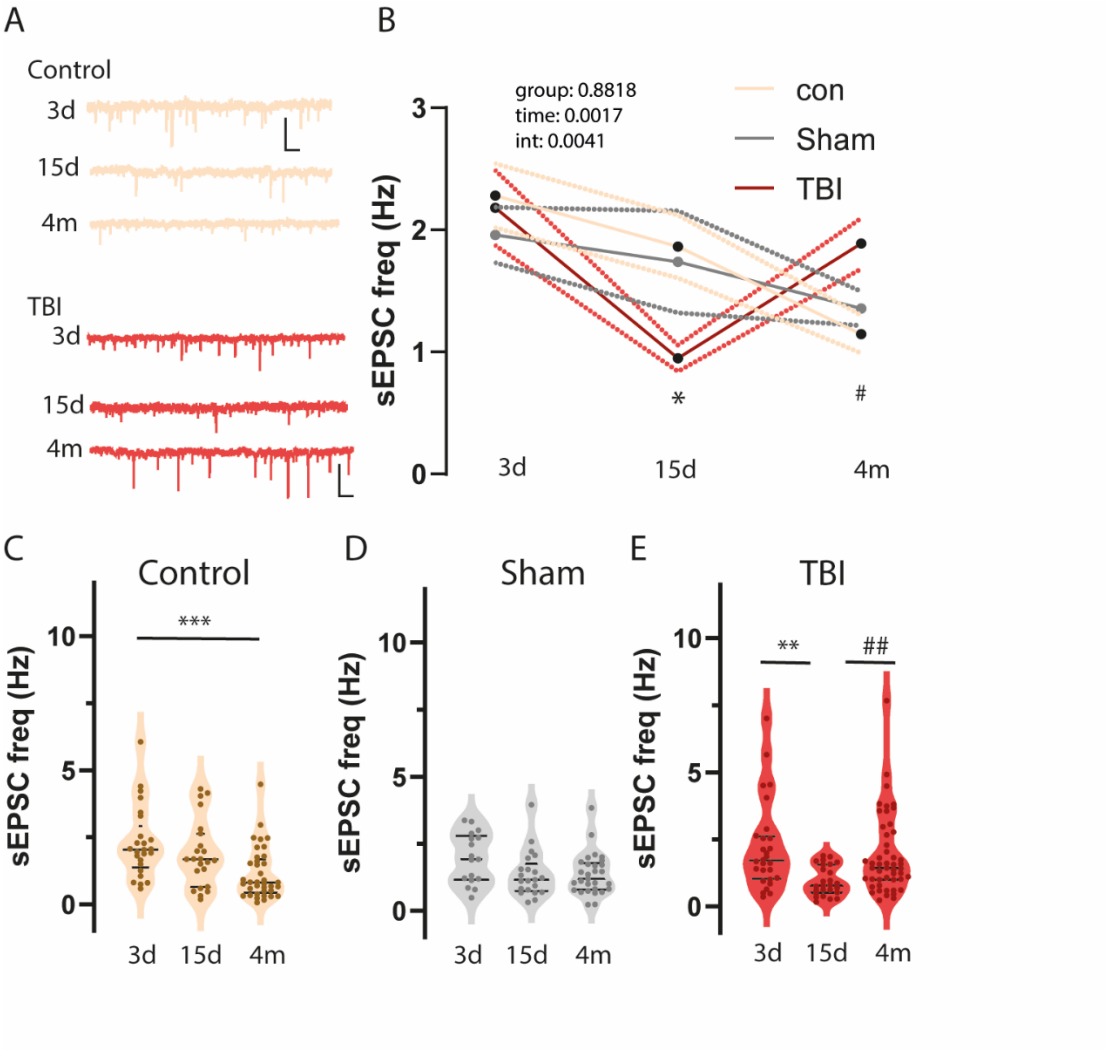

Figure 4. sEPSC frequency time course is disrupted by TBI

(**A**) Representative sEPSC traces from control (orange) and TBI (red) granule cells at day 3, day 15 and 4 months after surgery (Scale bar 20 pA, 500ms) (**B**) sEPSC frequency at the short- medium- and long-term for control (orange), Sham (gray) and TBI (red) granule cells (Two-way-ANOVA, group F (2, 247) = 0.1259, p = 0.8818; int F (4, 247) = 3.935, p= 0.004; time F(2, 247) = 6,522, p= 0.00171 *p= 0.0334 for TBI vs control and #p=0.0216 for TBI vs control in Dunn's multiple comparisons test). (**C**) sEPSC frequency in control cells at day 3 (n=25), day 15 (n=23) and 4 months (n=37) after surgery (Kruskal-Wallis test, H(2)= 14.67,p=0.0007, ***p=0.0005 for month 4 vs day 3 in Dunn's multiple comparisons test). (**D**) sEPSC frequency in Sham cells at day 3 (n=17), day 15 (n=21) and 4 months (n=29) after surgery. (**E**) sEPSC frequency in TBI cells at day 3 (n=28), day 15 (n=26) and 4 months (n=49) after surgery (Kruskal-Wallis test, H(2)= 13.87,p=0.0010, **p=0.0013 for day 15 vs day 3 and ##p=0.0075 for 4 months vs 15 days in Dunn's multiple comparisons test). For line graphs dots represent group means and area fill represents SEM. Dots in violin plots represent cell median values and dashed lines quartiles and group medians.

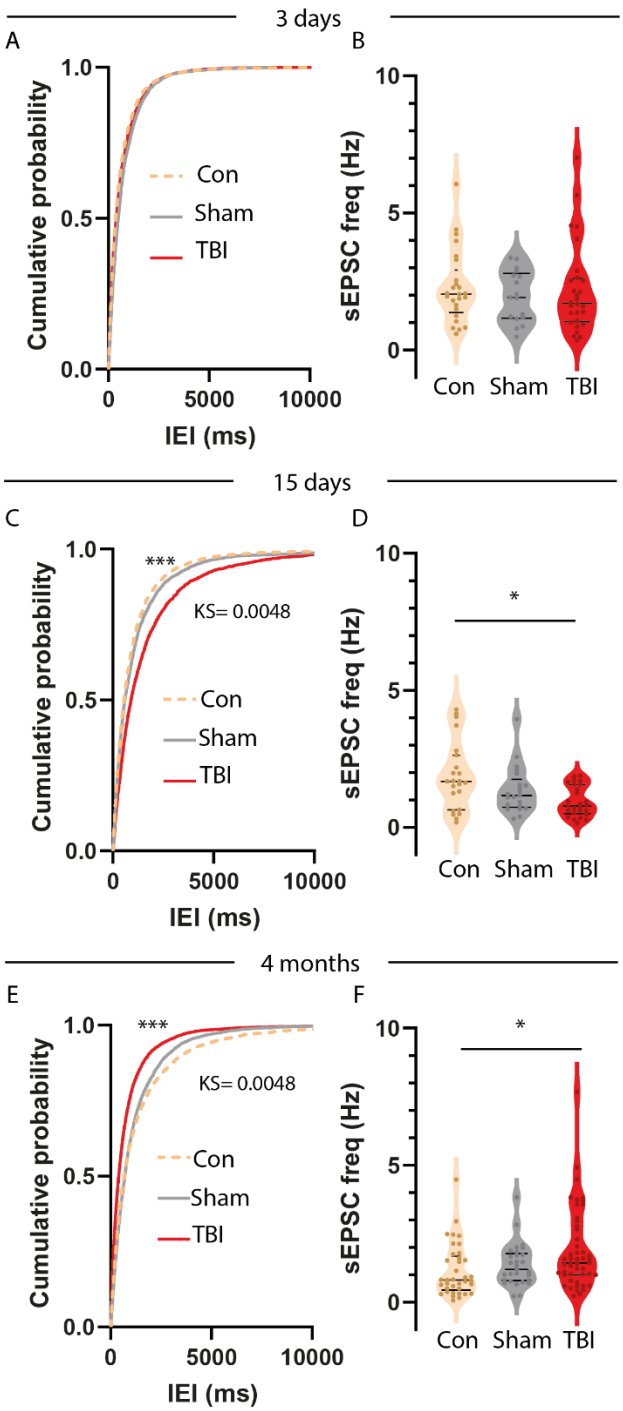

Figure 5. TBI impairs frequency of sEPSC at the medium- and long-term

(**A-B**) Cumulative probability plots of inter-event interval (IEI) (A) and violin plots showing sEPSC amplitudes (B) for control (orange), Sham (gray) and TBI (red) granule cells at day 3 after the surgery (n=25 for control, n= 17 for Sham and n= 28 for TBI). (**C-D**) Cumulative probability plots of IEI (C) and sEPSC frequency violin plots (D) for control (orange), Sham (gray) and TBI (red) granule cells at day 15 after the surgery. (n=23 for control, n= 22 for Sham and n= 26 for TBI. Kruskal-Wallis test, H(2)= 7.792, p=0.0203, *p= 0.0163 for TBI vs control in Dunn's multiple comparisons test). (**E-F**) Cumulative probability plots of IEI (E) and sEPSC frequency violin plots (F) for control (orange), Sham (gray) and TBI (red) granule cells 4 months after the surgery (n=37 for control, n=

29 for Sham and n= 49 for TBI. Kruskal-Wallis test, H(2)= 8.164, p=0.0169, *p= 0.0129 for TBI vs control in Dunn's multiple comparisons test). Dots in violin plots represent cell median values and dashed lines quartiles and group medians.

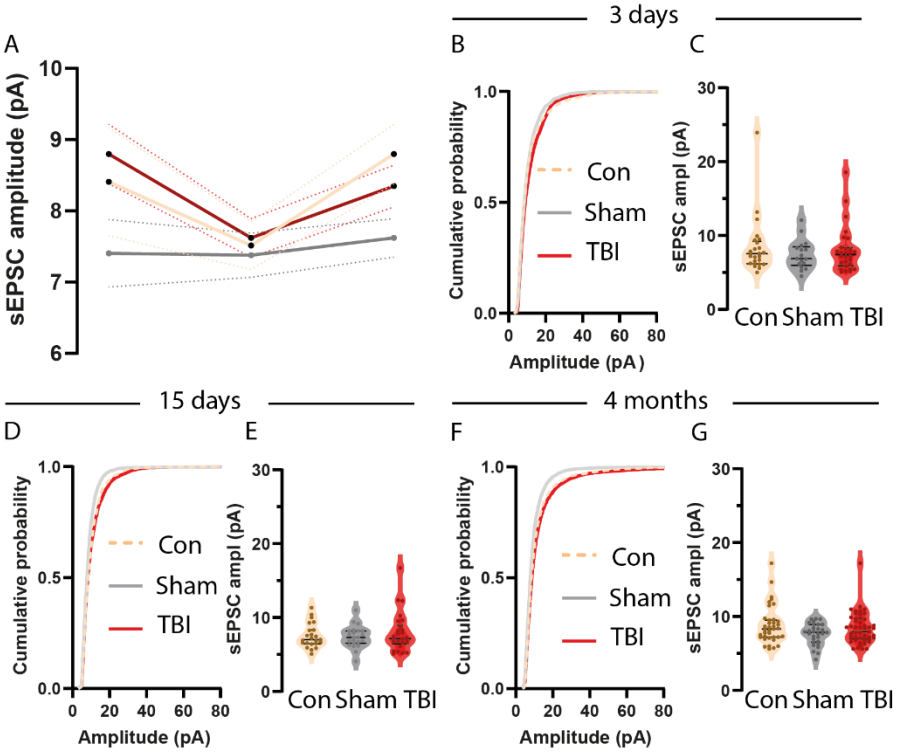

Figure 6. TBI does not affect amplitude of sEPSC at the short-, medium- and long-term.

(**A**) sEPSC amplitude at the short- medium- and long-term for control (orange), Sham (gray) and TBI (red) granule cells (**B**) sEPSC amplitude at the short- medium- and long-term for control (orange), Sham (gray) and TBI (red) granule cells. (**B-C**) Cumulative probability plots of sEPSC amplitude (IEI) (B) and violin plots showing sEPSC amplitudes (C) for control (orange), Sham (gray) and TBI (red) granule cells at day 3 after the surgery (n=25 for control, n= 17 for Sham and n= 28 for TBI). (**D-E**) Cumulative probability plots of sEPSC amplitude (D) and violin plots showing sEPSC amplitudes (E) for control (orange), Sham (gray) and TBI (red) granule cells at day 15 after the surgery. (n=23 for control, n= 22 for Sham and n= 26 for TBI. (**F-G**) Cumulative probability plots of sEPSC amplitude (F) and violin plots showing sEPSC amplitudes (G) for control (orange), Sham (gray) and TBI (red) granule cells 4 months after the surgery (n=37 for control, n= 29 for Sham and n= 49 for TBI). For line graphs dots represent group means and area fill represents SEM. Dots in violin plots represent cell median values and dashed lines quartiles and medians.

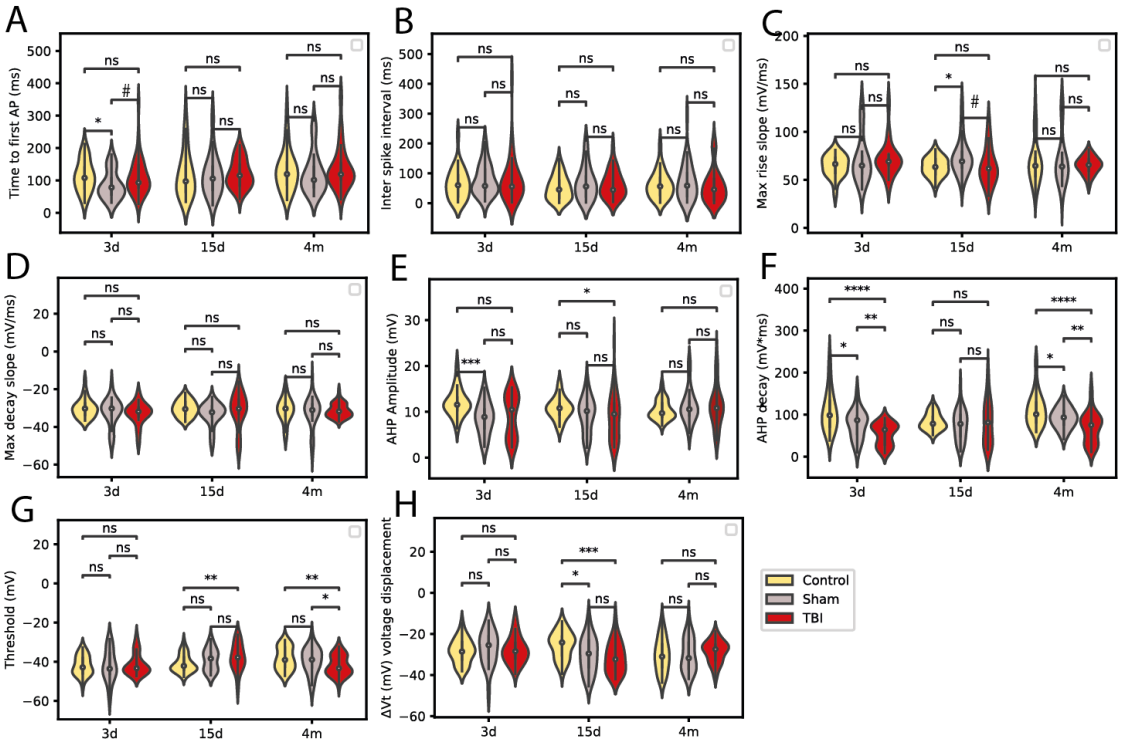

Supplementary figure 1. Action potential properties of control, Sham and TBI granule cells at short- medium- and long-term.

(**A**) Time to first action potential (AP) in control (orange), Sham (gray) and TBO (red) granule cells at day 3, day 15 and 4 months after the surgery. (**B**) Inter-spike interval in control (orange), Sham (gray) and TBO (red) granule cells at day3, day 15 and 4 months after the surgery. (**C**) Maximum rise slope in control (orange), Sham (gray) and TBO (red) granule cells at day3, day 15 and 4 months after the surgery. (**D**) Maximum decay slope in control (orange), Sham (gray) and TBO (red) granule cells at day3, day 15 and 4 months after the surgery. (**E**) Afterhyperpolarization (AHP) amplitude in control (orange), Sham (gray) and TBO (red) granule cells at day3, day 15 and 4 months after the surgery. (**F**) AHP decay in control (orange), Sham (gray) and TBO (red) granule cells at day3, day 15 and 4 months after the surgery. (**G**) AP threshold in control (orange), Sham (gray) and TBO (red) granule cells at day3, day 15 and 4 months after the surgery. (**H**) Voltage displacement in control (orange), Sham (gray) and TBO (red) granule cells at day3, day 15 and 4 months after the surgery. n=14 neurons from control; 25 from Sham and 38 from TBI at day 3; n=35 neurons from control; 35 from Sham and 37 from TBI at day 15; n=43 neurons from control; 34 from Sham and 64 from TBI at 4 months. Dots in violin plots represent group medians and lines SD.

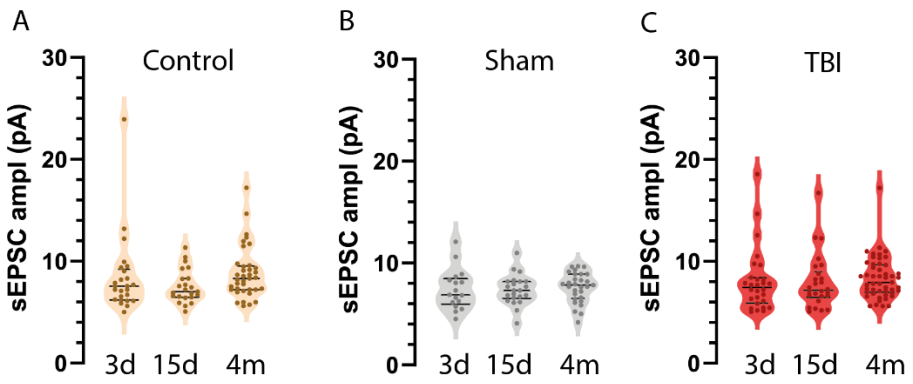

Supplementary figure 2. Amplitude of sEPSC remains stable in the three groups at the short-, medium- and long-term.

(**A**) sEPSC amplitude in control cells at day 3 (n=25), day 15 (n=23) and 4 months (n=37) after surgery. (**B**) sEPSC amplitude in Sham cells at day 3 (n=17), day 15 (n=21) and 4 months (n=29) after surgery. (**C**) sEPSC amplitude in TBI cells at day 3 (n=28), day 15 (n=26) and 4 months (n=49) after surgery. Dots in violin plots represent cell median values and dashed lines quartiles and medians.